HHS Public Access

Author manuscript

JACC Clin Electrophysiol. Author manuscript; available in PMC 2020 October 01.

Published in final edited form as:

JACC Clin Electrophysiol. 2019 October ; 5(10): 1158–1167. doi:10.1016/j.jacep.2019.06.017.

Epicardial Conduction Speed, Electrogram Abnormality and Computed Tomography Attenuation Associations in Arrhythmogenic Right Ventricular Cardiomyopathy

Tuna Ustunkaya, MD, PhD[a], **Benoit Desjardins, MD, PhD**[b], **Riley Wedan**[a], **C. Anwar A. Chahal, MB ChB, PhD**[a], **Stefan L. Zimmerman, MD**[c], **Nissi Saju, MSN**[d], **Sohail Zahid, PhD**[e], **Apurva Sharma, MD**[d], **Yuchi Han, MD**[e], **Natalia Trayanova, PhD**[f], **Francis E. Marchlinski, MD**[a], **Hugh Calkins, MD**[d], **Harikrishna Tandri, MD**[d], **Saman Nazarian, MD, PhD**[a]

[a.]Cardiac Electrophysiology, Hospital of the University of Pennsylvania, Philadelphia, PA

[b.]Department of Radiology, Hospital of the University of Pennsylvania, Philadelphia, PA

[c.]Radiology, Johns Hopkins University School of Medicine, Baltimore, M

[d.]Cardiac Electrophysiology, Johns Hopkins University School of Medicine, Baltimore, MD

[e.]Cardiovascular Division, Hospital of the University of Pennsylvania, Philadelphia, PA

[f.]Biomedical Engineering, Johns Hopkins University, Baltimore, MD

Abstract

Objective: We sought to evaluate the association between contrast-enhanced MDCT (CE-MDCT) attenuation and local epicardial conduction speed (ECS) and electrogram abnormalities in patients with arrhythmogenic right ventricular cardiomyopathy (ARVC) and ventricular tachycardia (VT).

Background: CE-MDCT is a widely available and fast imaging technology with high spatial resolution and less prone to defibrillator generator related safety issues and image artifacts. However, the association between hypoattenuation on MDCT and VT substrates in ARVC remains unknown.

Methods: Patients with ARVC that underwent CE-MDCT followed by endocardial (n=30) and epicardial (n=21) electroanatomical mapping (EAM) and VT ablation were prospectively enrolled. Right ventricular mid-myocardial attenuation was calculated from 3D MDCT images and

Corresponding author: Saman Nazarian MD, PhD, University of Pennsylvania Perelman School of MedicineCardiac Electrophysiology Section, 3400 Spruce Street/Founders 9, Philadelphia, PA 19143, saman.nazarian@uphs.upenn.edu, Phone: +1 (215) 615-5220 | Fax: + 1 (215) 615-5235.

Disclosures: Dr. Nazarian is a consultant for St Jude Medical, Siemens, Biosense Webster, and CardioSolv, and serves as PI for research funding from Biosense Webster, Imricor, and Siemens. The University of Pennsylvania Conflict of Interest Committee manages all commercial arrangements.

registered to EAM. Local ECS was calculated by averaging the ECS between each point and five adjacent points with concordant wave-front direction.

Results: A total of 17,311 epicardial and 5,204 endocardial points were included. In multivariable regression analysis clustered by patient, RV myocardial attenuation was associated with epicardial bipolar voltage amplitude (2.5% decrease in amplitude per 10 HU decrease in attenuation, p<0.001), with endocardial unipolar voltage amplitude (0.9% decrease in amplitude per 10 HU decrease in attenuation, p<0.001), and with ECS (0.4% decrease in ECS per 10 HU decrease in attenuation, p=0.001).

Conclusion: CE-MDCT attenuation distribution is associated with regional ECS and electrogram amplitude in ARVC. Regions with low attenuation likely reflect fibro-fatty involvement in the right ventricle and may serve as important VT substrates in ARVC patients undergoing VT ablation.

Condensed abstract

Arrhythmogenic right ventricular cardiomyopathy (ARVC) is characterized by fibro-fatty myocardial replacement. Identification of this arrhythmic substrate using imaging is useful for guidance of ventricular tachycardia (VT) ablation. In this study we demonstrate that hypoattenuated areas on contrast-enhanced multidetector computed tomography (CE-MDCT) are associated with abnormal epicardial bipolar voltage amplitude, and endocardial unipolar and bipolar voltage amplitudes, with decreasing strength of association, respectively. Pre-operative recognition of hypoattenuated CE-MDCT regions as important VT substrates, may result in improved strategies for VT ablation in ARVC patients.

Keywords

conduction speed; multi-detector computed tomography; ventricular tachycardia ablation; arrhythmogenic right ventricular cardiomyopathy; epicardial mapping; endocardial mapping

Introduction:

Arrhythmogenic right ventricular cardiomyopathy (ARVC) is characterized by fibro-fatty replacement predominantly involving the right ventricle, arrhythmias and sudden death (1). Catheter ablation is effective in ameliorating the frequency of arrhythmias (2). However, given the patchy distribution of disease, sampling density limitations, and intramural/epicardial nature of VT circuits, endocardial mapping and ablation can be challenging. Additionally, epicardial electroanatomical mapping (EAM) can be limited by fat deposition and myo-pericardial adhesions. Therefore, approaches to augment substrate identification are desirable. Cardiac magnetic resonance (CMR) allows visualization of anatomic and dynamic right ventricular (RV) abnormalities, fat infiltration and fibrosis (3–5). Compared to CMR, multidetector computed tomography (MDCT) has higher spatial resolution, shorter acquisition time, and is widely available with minimal image degradation or safety issues associated with implanted defibrillators (6,7). Contrast-enhanced MDCT (CE-MDCT) detects intramyocardial fat (8), epicardial fat (9), RV trabeculation and RV wall bulging (10) providing additional value in the diagnosis of ARVC. Moreover, the extent and location of fat and low-voltage epicardial areas are strongly associated (11). Preprocedural MDCT

review and integration may impact epicardial access plans, and targets for dense mapping and ablation (12). In this study, we sought to demonstrate the point by point association between MDCT attenuation, epicardial conduction speed (ECS) and endocardial/epicardial voltage abnormalities in patients with ARVC that underwent VT ablation.

Methods:

Patient cohort

The Johns Hopkins University and the University of Pennsylvania Perelman Schools of Medicine Institutional Review Boards approved the study protocol and all patients provided written informed consent. Thirty patients who met 2010 Revised Task Force criteria (4) for ARVC and underwent VT ablation as a part of the Ancillary Study of Substrate and Intervention Mechanisms for Ventricular Tachycardia (AIM-VT) cohort were prospectively enrolled. The ARVC Task Force Criteria for patients are summarized in Supplemental Table 1. All patients had endocardial mapping, and 21 patients also underwent epicardial mapping (70%). Operators were blinded to attenuation data from CE-MDCT.

CE-MDCT acquisition

CE-MDCT images were obtained using a Toshiba Aquillion 320-slice MDCT system during breath-hold to detect first pass perfusion. The median duration from pre-operative CE-MDCT to ablation procedure was 0 days for all patients (IQR 0–0, range 0–63 days). Bolus triggering based on attenuation in the descending aorta was utilized with the settings of (dFOV: 200–220, range: 128–140 mm, gantry rotation 0.275 ms, tube voltage 80–120 kV). Contrast (Isovue-370 in 14, Visipaque in 1; 70–80 cc) was administered through a right arm 18 gauge IV, at 4–5 ml/sec depending on the patient weight using the following sequence (1) 45–65 cc contrast injection (depending on the tube voltage and patient weight); (2) 40 cc of, 50/50 contrast/saline injection; and (3) 30cc of 100% saline flush. The scan was triggered manually by the cardiac CT technologist when the contrast bolus reached the descending thoracic aorta, typically 250 Hounsfield units. Images were acquired every 5% of the R-R interval and phases with least motion were used. Images were reconstructed using myocardium-optimized reconstruction kernels including beam hardening artifact correction (thickness 0.5 – 3 mm).

Electroanatomic Mapping

Endocardial EAM (n=30) was performed using either Thermocool SF or Thermocool Smart Touch SF ablation catheter (n=26, 87.7%) or by PENTARAY multielectrode catheter (n=4, 13.3%) and the the CARTO3 software. Epicardial access and EAM was performed, at physician’s discretion, using a Thermocool SF or Thermocool Smart Touch SF ablation catheter (n=7), multipolar PENTARAY catheter (n=13) or DECANAV catheter (n=1) (CARTO, Biosense Webster, Diamond Bar, CA). Detailed epicardial EAM focused on the entire RV and extended over the LV surface during sinus rhythm with intrinsic conduction or RV pacing. Bipolar and unipolar electrograms were filtered at 10 to 400 Hz and 1 to 240 Hz, respectively. Peak to peak signal amplitude and timing to the maximum signal dv/dt with reference to the surface QRS complex was measured automatically and confirmed manually

during the review. Catheter stability was confirmed using sharp deflections on two consecutive beats.

CE-MDCT registration with EAM

The RV border was created using the volume rendering function of ADAS-3D (Galgo Medical, Barcelona, Spain). After volume rendering, the RV border was visually dilated by 1 mm in order to avoid blood pool artifact, while taking care to avoid hypo attenuated regions (<−180 HU) indicative of epicardial fat. The volume rendering and contouring process are illustrated in Figure 1A–B. High intensity regions (> 200 HU) surrounding ICD electrodes were manually excluded (Figure 1C). Images were then 3D reconstructed and exported for EAM registration. 3D reconstructed MDCT shells were registered with endocardial maps using tricuspid annulus, RV outflow tract and apex as landmarks (Supplemental Figure 1). Merged images were then re-imported to ADAS3D, whereby the attenuation of each EAM point was calculated using trilinear interpolation of the closest region on the CT shell. Epicardial points detected to be on the LV side were deleted using the ADAS3D software.

Points close to the tricuspid annulus, which project to the blood pool with > 200 HU attenuation, as well as points that projected to epicardial fat with < −180 HU attenuation values, were excluded. The mean distance of EAM points to the RV endocardium was 6.1 ± 4.4 mm (1.4 between-patient and 3.9 within-patient SD). The mean distance to the RV epicardium was 5.1 ± 4.3 mm (1.8 between-patient SD and 3.9 within-patient SD).

Epicardial Conduction speed analyses

The ECS was calculated with a custom script written in Python (https://www.python.org) (13). First, the EAM file of activation times and x,y,z spatial coordinates of each point are imported into the software. The algorithm creates a KD tree, which is a specialized data structure that efficiently stores spatial location, so that the closest point coordinates can be queried in a fast manner (specifically N log N time). It retrieves all the spatial coordinates and activation times that are nearby a specific data point and ignores duplicates. The software then calculates the distance between EAM points using x,y,z coordinates, and calculates the time differences between points using differences of activation times from the fiducial electrogram during data acquisition. Activation fronts are then assessed based upon heterogeneity of nearby activation times. Nearby points with a difference in local activation time <5 ms from the index point are considered to be activated along a different wave front and excluded from the conduction speed calculation for that index point. Conduction speed is then calculated as the average distance divided by time. Regional conduction speed is calculated by averaging the conduction speed of five adjacent points along the activation front. Lastly, the software outputs the conduction speed data into a text file. The Python script has been submitted as supplementary material. This methodology has previously been validated (13–17).

Statistical analyses

Continuous variables are expressed as mean ± SD or median and interquartile range. Categorical variables are expressed as % change. Because of the right-skewed nature of bipolar, unipolar, and ECS data, logarithmic transformation was performed. To examine the

association between attenuation and other variables, a multilevel random effects linear regression model clustered by patient was used. If logarithmic conversion was performed, the correlation coefficient was recognized to reflect the ratio of change instead of actual arithmetic change. Thus, all the correlation coefficients between independent variables and logarithmically converted dependent variable were expressed as percent change in the dependent variable. All statistical analyses were performed using STATA software version 15 (College Station, TX).

Results:

Patient Characteristics

The cohort consisted of 30 patients (age 39 ± 15 years, 57% female, 83% non-Hispanic white) with ARVC that underwent VT ablation. All patients underwent endocardial mapping, and 21 patients (70%) underwent concomitant epicardial mapping and ablation. The mean age of patients that underwent epicardial ablation was 37.6 ± 14.8 years, 57% were female, and 90% were Caucasian.

Association of CE-MDCT attenuation with endocardial voltage

Of 6,336 endocardial mapping points 853 (13.4%) corresponded to areas with ICD artifact, 245 (3.8%) to endocardial blood pool and 34 (0.5%) to the areas of epicardial fat and were excluded. The remaining 5,204 (median 129, IQR (82 – 157) from 30 patients were registered to image data and used for analysis. The mean unipolar voltage amplitude was 3.59 ± 2.68 mV (1.06 between-patient and 2.54 within-patient SD). The mean bipolar voltage amplitude was 1.99 ± 2.36 mV (0.85 between-patient and 2.25 within-patient SD). The mean RV myocardial attenuation on CE-MDCT corresponding to the endocardial points was 40.1 ± 70.3 HU (26.1 between-patient and 67.6 within-patient SD).

In the patient clustered linear regression model, bipolar electrogram amplitude was associated with RV myocardial attenuation (0.7% decrease in bipolar voltage per 10 HU decrease in attenuation; 95% CI: 0.3–1.1%, p=0.001). Unipolar electrogram amplitude had a stronger magnitude of association with RV myocardial attenuation (0.9% decrease in unipolar voltage per 10 HU decrease in attenuation; 95% CI: 0.7%−1.2%, p<0.001). Associations between MDCT attenuation, bipolar voltage amplitude, and unipolar voltage amplitude did not change significantly after adjusting for age, gender, ethnicity, and patient weight. Figure 2 demonstrates the association between endocardial bipolar and unipolar voltage amplitude measurements and RV myocardial attenuation. Consistent with the statistical associations above, the images reveal a closer association between CT attenuation and endocardial unipolar measurements, when compared to endocardial bipolar measurements, which appear to diverge from attenuation measurements in the antero-apical RV.

Association of CE-MDCT attenuation with epicardial voltage and ECS

Of 19,360 epicardial mapping points, 1,662 points (8.5%) corresponded to areas with ICD artifact, 159 (0.8%) to the epicardial fat, and 228 (1.1%) to the endocardial blood pool. The remaining 17,311 points (median 885, IQR (229, 1517) from 21 patients were registered to

image data and used for analysis. The mean ECS was 0.37 ± 0.33 m/s (0.23 between-patient and 0.30 within-patient SD). The mean unipolar voltage amplitude was 2.69 ± 3.5 mV (0.82 between-patient and 3.42 within-patient SD). The mean bipolar voltage amplitude was 1.07 ± 3.48 mV (0.39 between-patient and 1.43 within-patient SD). The mean RV myocardial attenuation on CE-MDCT corresponding to the epicardial points was 8.8 ± 73.6 HU (23.7 between-patient and 69.4 within-patient SD).

In the patient clustered linear regression model, bipolar electrogram amplitude was associated with RV myocardial attenuation (2.5% decrease in bipolar voltage per 10 HU decrease in attenuation; 95% CI: 2.2%−2.7%, p<0.001). The magnitude of association between epicardial unipolar electrogram amplitude and RV myocardial attenuation was smaller (0.8% decrease in amplitude per 10 HU decrease in attenuation, 95% CI: 0.7% −0.9%, p<0.001). RV myocardial attenuation was also significantly associated with local ECS (0.4% decrease in ECS per 10 HU decrease in attenuation, 95% CI: 0.2%−0.6%, p=0.001). Local ECS was strongly associated with both epicardial bipolar (1.9% decrease in ECS per 1 mV decrease in amplitude, 95% CI: 1.4%−2.3%) and epicardial unipolar voltage amplitude (2.5% decrease in ECS per 1 mV decrease in amplitude, 95% CI: 2%−3%). Figure 3 shows the association between epicardial bipolar voltage amplitude and RV myocardial attenuation. It is evident from these images that CT attenuation is closely associated with epicardial bipolar amplitude measurements. Consequently, ablation, which was guided by abnormal electrograms and entrainment was confined to low attenuation regions on CE-MDCT despite the fact that operators were blinded to CT attenuation data. Examples of lesion sets relative to attenuation images have been provided in Figure 4.

Association of CE-MDCT attenuation with binned regionality of scar assessment by voltage

Regional analysis of points binned as normal voltage zone amplitude (defined as epicardial voltage amplitude >1 mV) versus epicardial border-zone voltage amplitude (defined as epicardial voltage amplitude >0.5 mV and <1 mV) and epicardial scar (defined as epicardial voltage amplitude <0.5 mV) revealed significant association with RV myocardial attenuation on CE-MDCT (p<0.001). Similarly, abnormal endocardial unipolar voltage amplitude (defined as RV <5.5 mV) was significantly associated with the CE-MDCT RV myocardial attenuation (p=0.006). However, in binned regional analyses, the endocardial bipolar voltage amplitude failed to show a significant association with RV myocardial attenuation (p=0.132). The mean attenuation for each region is summarized in Supplemental Table 2.

Discussion:

The present study highlights regional RV associations between low attenuated areas reflecting intramyocardial fat deposition and: 1) epicardial bipolar voltage abnormalities; 2) endocardial unipolar and, to a lesser degree, bipolar voltage abnormalities; and 3) conduction speed. These findings are discussed below.

Contrast-enhanced MDCT in ARVC

Contrast-enhanced CT refers to the protocol that of immediate imaging following contrast perfusion into the chamber of interest. While both contrast-enhanced CT and non-contrast CT are capable of fat identification as very low attenuation regions, contrast-enhanced CT allows for better visualization of ventricular myocardial borders and enables the identification of fibrotic regions due to reduced immediate tissue perfusion and contrast uptake, thus lower attenuation in such regions (6,18). Additionally, CE-MDCT provides highly reproducible measurements of attenuation (19). Fibro-fatty infiltration is, therefore, characterized by low-attenuation CE-MDCT regions in ARVC patients (11,12). Endocardial unipolar voltage mapping is utilized to identify arrhythmogenic ARVC substrate but is limited by reduced specificity (20), and epicardial ablation results in improved outcomes due to improved substrate detection and elimination in ARVC (21). Our data demonstrates that endocardial unipolar and epicardial bipolar electrogram amplitudes are strongly associated with low attenuation areas, as a surrogate of intramyocardial fat deposition and provide an alternative methodology for substrate identification. Targeting of such low attenuation substrates may improve endocardial ablation outcomes.

Slow conduction speed has been shown to be an important indicator of myocardial fibrosis in atrial and ventricular tissue (13,17). The current study demonstrates that epicardial conduction speed is associated with ARVC related fibro-fatty metaplasia and may identify important targets in substrate mapping for VT ablation. Fat deposition and fibrosis co-exist in abnormal ARVC myocardium, and both contribute to arrhythmogenesis (22). The current study did not attempt to segment the hypo-attenuated substrate, and instead depicted the association between hypoattenuated areas with voltage and low conduction speed. We did not distinguish between fat and fibrosis because histologic data to delineate accurate thresholds are unavailable. However, based upon prior studies, very low attenuation regions exhibiting values between −80 to 0 HU appear to indicate fat, with different studies suggesting −10 and - 20 HU as threshold values (7,8,11,23). In contrast, fibrosis appears to have slightly higher attenuation with values between 0 – 30 HU representative of LV fibrosis in post-MI patients. (24,25) Regardless, without additional imaging modalities, distinction between fat and fibrosis cannot be made with certainty. It is also important to note that despite an overall strong association between CE-MDCT attenuation and ECS, 6% of the slow conducting zones (defined as ECS <0.3 m/s) in this study corresponded to areas with bipolar voltage amplitude ≥ 1.5 mV and normal attenuation. Thus, not all ECS heterogeneity is attributable to tissue heterogeneity as detected by CE-MDCT and may be due to other factors including uncoupling and anisotropic conduction or variability in wall thickness and source/sink mismatch.

This is the largest prospective study evaluating the difference between endocardial and epicardial, EAM in ARVC and their association with CE-MDCT. We demonstrate the associations using a point by point approach rather than a regional approach employed by previous studies. Epicardial voltage maps demonstrated a much stronger association with image attenuation compared to endocardial maps, providing further evidence that ARVC is characterized by a primary epicardial substrate.

Study Limitations

This was a single center study with a small sample size and may be prone to selection bias and reduced generalizability. Nevertheless, the study had a relatively larger sample size than prior studies on image and electrogram associations in ARVC. A significant number of patients had ICDs implanted which might affect the evaluation of right ventricular apex and right ventricular free wall. Electrograms were predominantly sampled during sinus rhythm. However, in some patients, sampling was performed during RV pacing. The wave front of propagation may affect ECS. However, clustering of the analyses by patient adjusts for the effect of pacing which was differential only at the patient level. Due to the relatively low density of electrogram sampling in the endocardium, conduction speed measurements were not performed for that surface. Due to the thin nature of the RV wall, some contours may have included epicardial fat or blood pool and registration errors existed. Finally, epicardial mapping was predominantly performed using a multi-electrode catheter, whereas endocardial mapping was performed using an ablation catheter. Thus, epicardial maps had significantly higher point density. Endocardial mapping density was sparse on diseased regions, whereas epicardial maps had high density throughout the RV; therefore, the mean attenuation among sampled endocardium and epicardium points is not random. However, since all associations were performed at a point level, no significant bias is anticipated as a result of this surface-based density difference.

Supplementary Material

Refer to Web version on PubMed Central for supplementary material.

Funding:

The study was funded through NIH grants R01HL116280 and R01HL142893 to Dr. Nazarian, and NIH grant PD1HL123271 and a grant from Foundation Leducq to Dr. Trayanova. The contents do not necessarily represent the views of the National Institutes of Health.

Abbreviations

ARVC	Arrhythmogenic right ventricular dysplasia/cardiomyopathy
CE-MDCT	Contrast-enhanced multi-detector computerized tomography
CMR	cardiac magnetic resonance
ECS	epicardial conduction speed
EAM	Electroanatomical mapping
HU	Hounsfield Unit
ICD	Implantable cardioverter-defibrillator
IQR	Interquartile range
MDCT	multi-detector computerized tomography

LV	left ventricular
RV	right ventricular
VT	ventricular tachycardia

References

1. Thiene G, Nava A, Corrado D, Rossi L, Pennelli N. Right ventricular cardiomyopathy and sudden death in young people. N Engl J Med 1988;318:129–33. [PubMed: 3336399]
2. Souissi Z, Boule S, Hermida JS et al. Catheter ablation reduces ventricular tachycardia burden in patients with arrhythmogenic right ventricular cardiomyopathy: insights from a north-western French multicentre registry. Europace 2018;20:362–369. [PubMed: 28017936]
3. Sen-Chowdhry S, Prasad SK, Syrris P et al. Cardiovascular magnetic resonance in arrhythmogenic right ventricular cardiomyopathy revisited: comparison with task force criteria and genotype. J Am Coll Cardiol 2006;48:2132–40. [PubMed: 17113003]
4. Marcus FI, McKenna WJ, Sherrill D et al. Diagnosis of arrhythmogenic right ventricular cardiomyopathy/dysplasia: proposed modification of the task force criteria. Circulation 2010;121:1533–41. [PubMed: 20172911]
5. Deac M, Alpendurada F, Fanaie F et al. Prognostic value of cardiovascular magnetic resonance in patients with suspected arrhythmogenic right ventricular cardiomyopathy. Int J Cardiol 2013;168:3514–21. [PubMed: 23701935]
6. Tandri H, Bomma C, Calkins H, Bluemke DA. Magnetic resonance and computed tomography imaging of arrhythmogenic right ventricular dysplasia. J Magn Reson Imaging 2004;19:848–58. [PubMed: 15170788]
7. Cochet H, Denis A, Komatsu Y et al. Automated Quantification of Right Ventricular Fat at Contrast-enhanced Cardiac Multidetector CT in Arrhythmogenic Right Ventricular Cardiomyopathy. Radiology 2015;275:683–91. [PubMed: 25559233]
8. Kimura F, Matsuo Y, Nakajima T et al. Myocardial fat at cardiac imaging: how can we differentiate pathologic from physiologic fatty infiltration? Radiographics 2010;30:1587–602. [PubMed: 21071377]
9. Aliyari Ghasabeh M, Te Riele A, James CA et al. Epicardial Fat Distribution Assessed with Cardiac CT in Arrhythmogenic Right Ventricular Dysplasia/Cardiomyopathy. Radiology 2018:180224.
10. Nakajima T, Kimura F, Kajimoto K, Kasanuki H, Hagiwara N. Utility of ECG-gated MDCT to differentiate patients with ARVC/D from patients with ventricular tachyarrhythmias. J Cardiovasc Comput Tomogr 2013;7:223–33. [PubMed: 23992839]
11. Komatsu Y, Jadidi A, Sacher F et al. Relationship between MDCT-imaged myocardial fat and ventricular tachycardia substrate in arrhythmogenic right ventricular cardiomyopathy. J Am Heart Assoc 2014;3.
12. Yamashita S, Sacher F, Mahida S et al. Image Integration to Guide Catheter Ablation in Scar-Related Ventricular Tachycardia. J Cardiovasc Electrophysiol 2016;27:699–708. [PubMed: 26918883]
13. Fukumoto K, Habibi M, Ipek EG et al. Association of Left Atrial Local Conduction Velocity With Late Gadolinium Enhancement on Cardiac Magnetic Resonance in Patients With Atrial Fibrillation. Circ Arrhythm Electrophysiol 2016;9:e002897. [PubMed: 26917814]
14. Kistler PM, Sanders P, Fynn SP et al. Electrophysiologic and electroanatomic changes in the human atrium associated with age. J Am Coll Cardiol 2004;44:109–16. [PubMed: 15234418]
15. John B, Stiles MK, Kuklik P et al. Electrical remodelling of the left and right atria due to rheumatic mitral stenosis. Eur Heart J 2008;29:2234–43. [PubMed: 18621772]
16. Miyamoto K, Tsuchiya T, Narita S et al. Bipolar electrogram amplitudes in the left atrium are related to local conduction velocity in patients with atrial fibrillation. Europace 2009;11:1597–605. [PubMed: 19910315]
17. Ustunkaya T, Desjardins B, Liu B et al. Association of regional myocardial conduction velocity with the distribution of hypoattenuation on contrast-enhanced perfusion computed tomography in

patients with postinfarct ventricular tachycardia. Heart Rhythm 2019;16:588–594. [PubMed: 30935494]

18. Kimura F, Sakai F, Sakomura Y et al. Helical CT features of arrhythmogenic right ventricular cardiomyopathy. Radiographics 2002;22:1111–24. [PubMed: 12235341]
19. Stanton CL, Haramati LB, Berko NS et al. Normal myocardial perfusion on 64-detector resting cardiac CT. J Cardiovasc Comput Tomogr 2011;5:52–60. [PubMed: 21185253]
20. Polin GM, Haqqani H, Tzou W et al. Endocardial unipolar voltage mapping to identify epicardial substrate in arrhythmogenic right ventricular cardiomyopathy/dysplasia. Heart Rhythm 2011;8:76–83. [PubMed: 20933099]
21. Garcia FC, Bazan V, Zado ES, Ren JF, Marchlinski FE. Epicardial substrate and outcome with epicardial ablation of ventricular tachycardia in arrhythmogenic right ventricular cardiomyopathy/dysplasia. Circulation 2009;120:366–75. [PubMed: 19620503]
22. Marcus FI, Fontaine GH, Guiraudon G et al. Right ventricular dysplasia: a report of 24 adult cases. Circulation 1982;65:384–98. [PubMed: 7053899]
23. Tada H, Shimizu W, Ohe T et al. Usefulness of electron-beam computed tomography in arrhythmogenic right ventricular dysplasia. Relationship to electrophysiological abnormalities and left ventricular involvement. Circulation 1996;94:437–44. [PubMed: 8759086]
24. Sasaki T, Calkins H, Miller CF et al. New insight into scar-related ventricular tachycardia circuits in ischemic cardiomyopathy: Fat deposition after myocardial infarction on computed tomography--A pilot study. Heart Rhythm 2015;12:1508–18. [PubMed: 25814415]
25. Nieman K, Cury RC, Ferencik M et al. Differentiation of recent and chronic myocardial infarction by cardiac computed tomography. Am J Cardiol 2006;98:303–8. [PubMed: 16860013]

Perspectives:

ARVC patients frequently present with sustained VT and require catheter ablation to mitigate ICD shocks and symptoms. The arrhythmogenic substrate in ARVC is primarily epicardial and identification of the substrate near the atrioventricular or interventricular grooves can be difficult due to the preponderance of epicardial fat in such regions. In this study, we demonstrated that intramyocardial fat detected by CE-MDCT associates with electroanatomic abnormalities. Incorporation of CE-MDCT as an adjunct for mapping may augment ablation outcomes in ARVC patients.

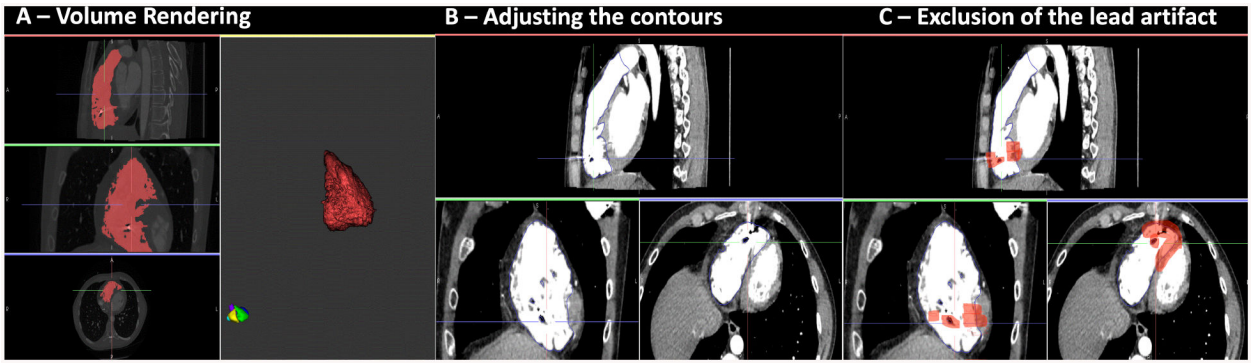

Figure 1. Segmentation Process

CE-MDCT, volume rendering, adjustment of segmentation contours, and exclusion of lead artifact areas. Panel A shows CE-MDCT in coronal, axial and sagittal views and creation of the 3D shell. Red highlighted areas have attenuation values >200 HU which represents blood pool. Panel B Shows representative cardiac contours in each image plane after contour adjustment. Panel C shows lead artifact exclusion (highlighted as red).

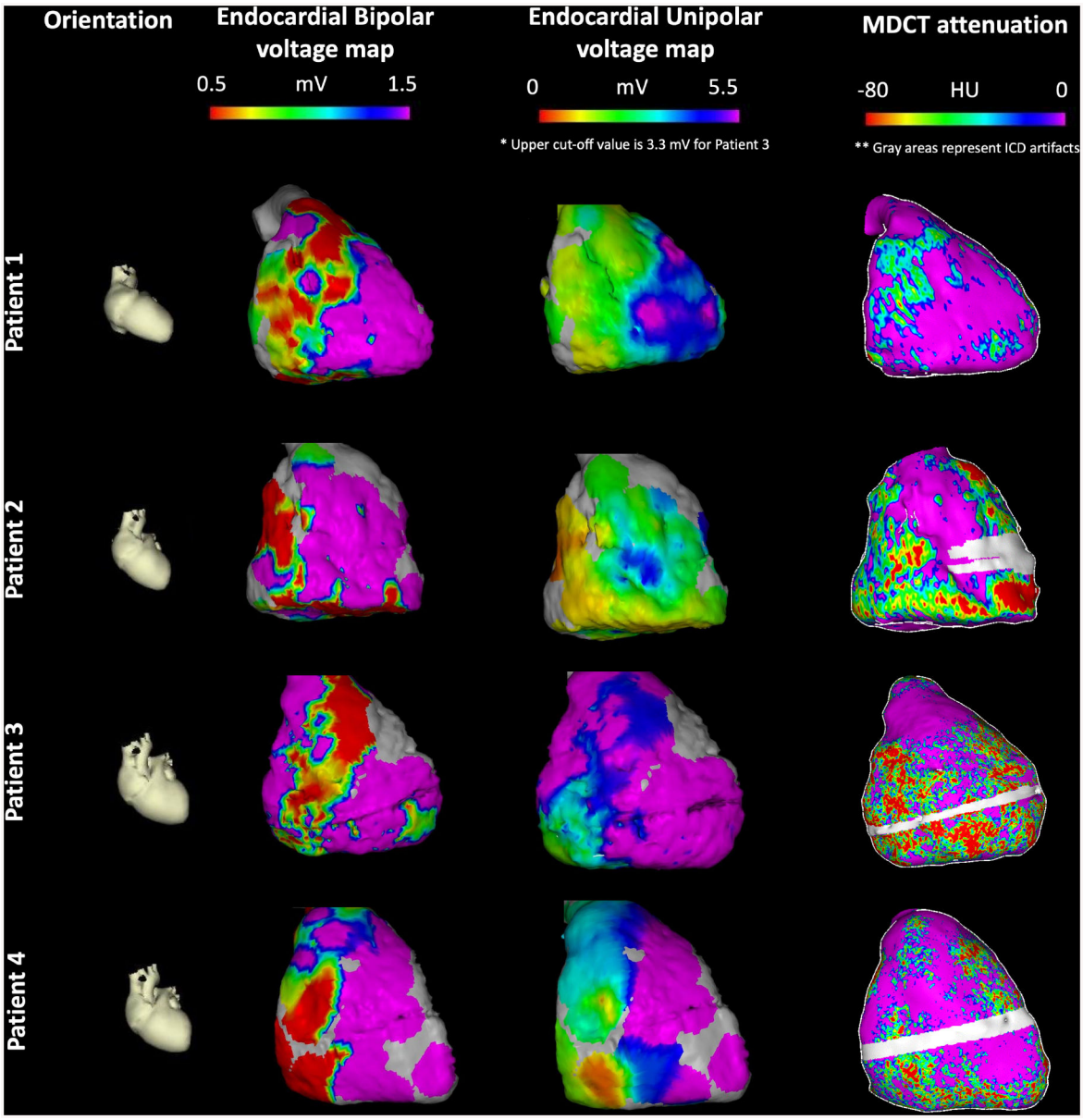

Figure 2. Endocardial bipolar and unipolar voltage vs. attenuation map examples

Each row represents a different patient. The first column shows cardiac orientation for the subsequent images in each row. The second column images display endocardial bipolar voltage maps projected onto the 3D MDCT shell. The third column images display endocardial unipolar voltage maps projected onto the 3D MDCT shell. Patient 3 had mapping using multi-electrode catheter hence upper cut-off of 3.3 mV was used for visualization. The fourth column images represent RV myocardial MDCT attenuation maps. The gray area in patients 2, 3 and 4 has been excluded due to ICD artifact.

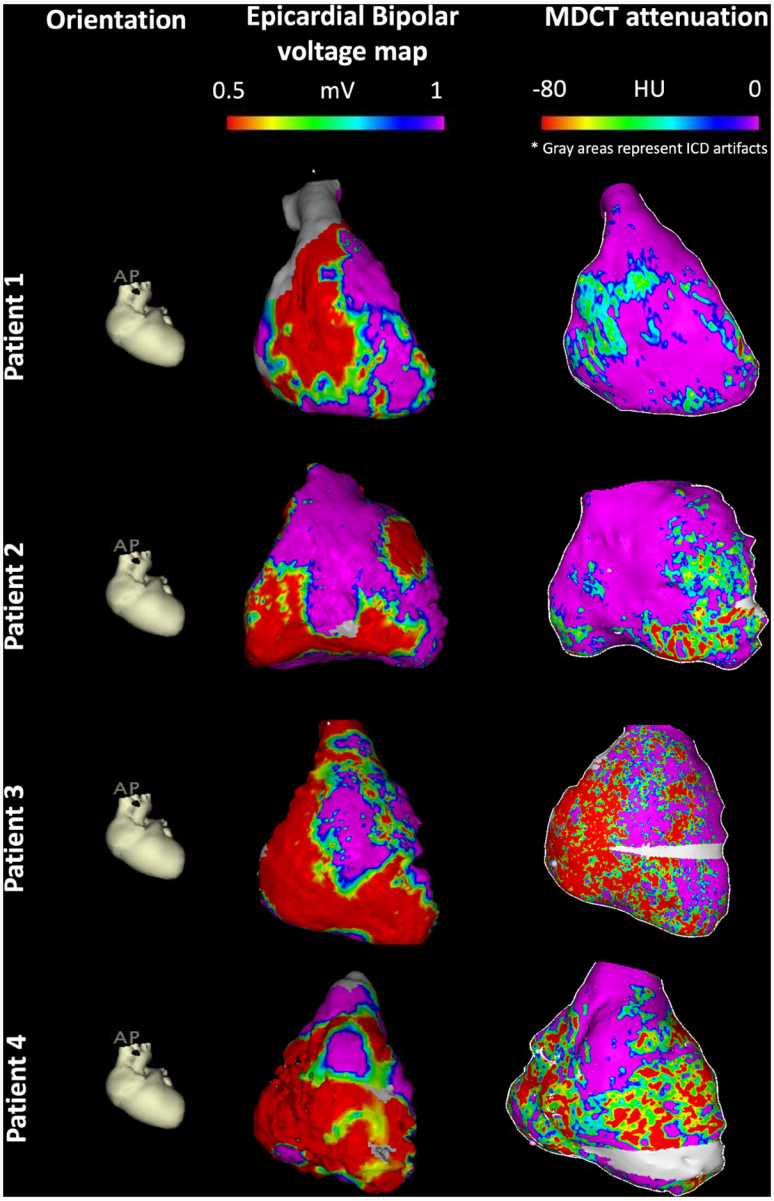

Figure 3. Epicardial Bipolar Voltage vs Attenuation Map examples

Each row represents a different patient. The first column shows cardiac orientation for the subsequent images in each row. The images in the second column represent epicardial bipolar voltage maps projected onto the 3D reconstructed shell from MDCT. Images in the third column represent RV myocardial MDCT attenuation maps. The gray area in patients 3 and 4 has been excluded due to ICD artifact. Of note, the resolution of MDCT attenuation maps are ~ 1000 point/cm^3, whereas the resolution of bipolar voltage electrograms is limited by the electroanatomic mapping density at ~ 1–6 point/cm^3 depending on the use of multi-electrode catheter versus point-by-point mapping.

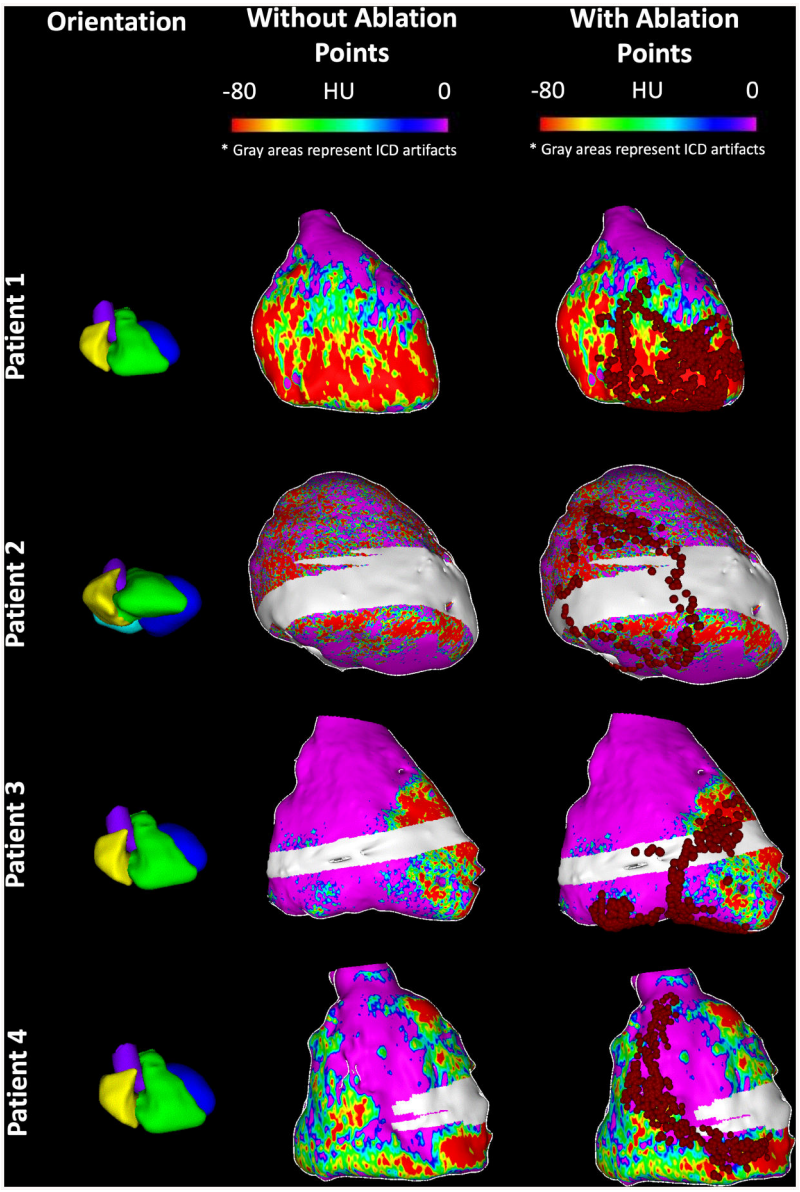

Figure 4. Association of ablation points with the attenuation maps.

Each row represents a different patient. The first column shows cardiac orientation for the subsequent images in each row. The second column shows CT attenuation values projected onto the 3D reconstructed shell from MDCT without ablation points. The third column represents the CT attenuation map from column 2 with ablation points superimposed as red dots. Gray areas on the shells represent regions with ICD artifact. Lesions were delivered within or at the periphery of regions with low attenuation on CE-MDCT in all cases.

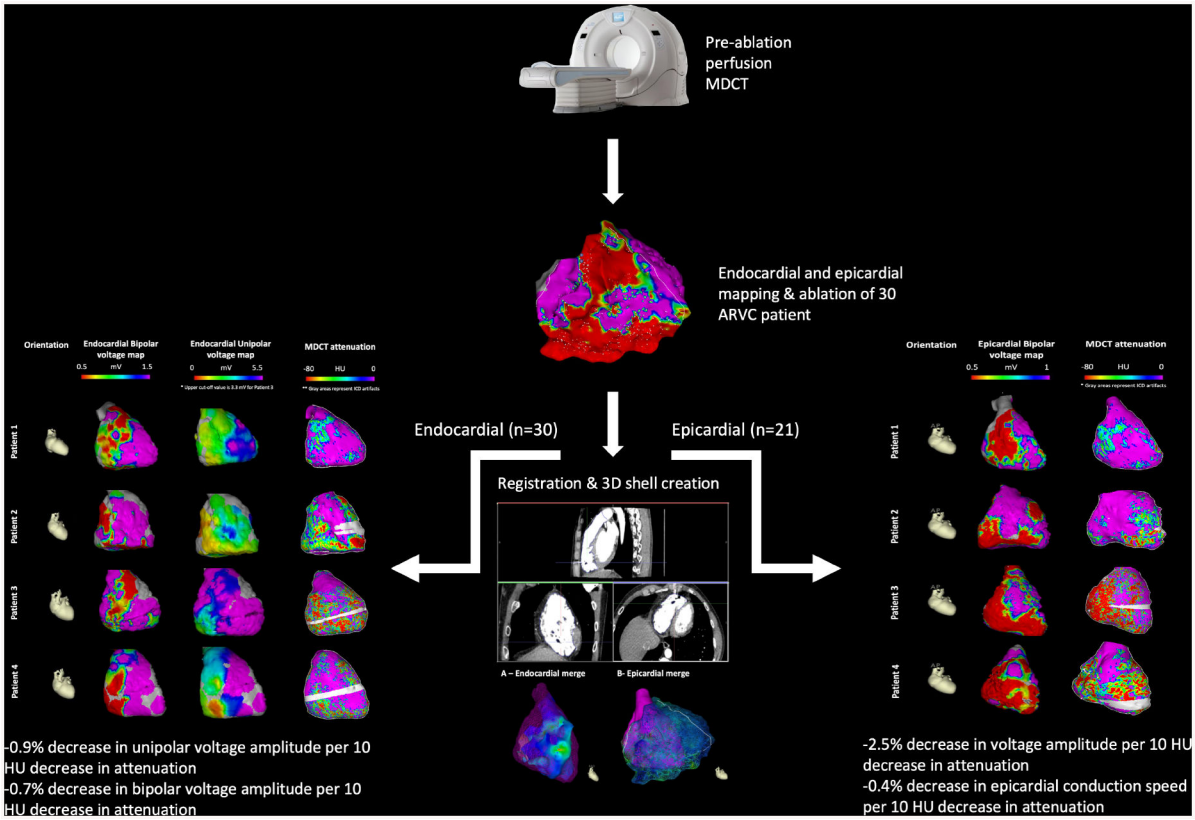

Central Illustration. AIM-VT-ARVC Study Protocol

Thirty patients with arrhythmogenic right ventricular cardiomyopathy (ARVC) underwent pre-procedural perfusion multidetector computed tomography (MDCT) followed by endocardial voltage mapping. Epicardial mapping was also performed in 70% of patients. Regional RV low image attenuation was associated with: 1) epicardial bipolar voltage abnormalities; 2) endocardial unipolar and, to a lesser degree, bipolar voltage abnormalities; and 3) conduction speed. 3D = 3-dimensional.